Measurements of Proton High Order Cumulants in $\sqrt{s_{\rm NN}} = 3$ GeV Au+Au Collisions and Implications for the QCD Critical Point

M. S. Abdallah[5], B. E. Aboona[55], J. Adam[6], L. Adamczyk[2], J. R. Adams[39], J. K. Adkins[30], G. Agakishiev[28], I. Aggarwal[41], M. M. Aggarwal[41], Z. Ahammed[61], I. Alekseev[3,35], D. M. Anderson[55], A. Aparin[28], E. C. Aschenauer[6], M. U. Ashraf[11], F. G. Atetalla[29], A. Attri[41], G. S. Averichev[28], V. Bairathi[53], W. Baker[10], J. G. Ball Cap[20], K. Barish[10], A. Behera[52], R. Bellwied[20], P. Bhagat[27], A. Bhasin[27], J. Bielcik[14], J. Bielcikova[38], I. G. Bordyuzhin[3], J. D. Brandenburg[6], A. V. Brandin[35], I. Bunzarov[28], X. Z. Cai[50], H. Caines[64], M. Calderón de la Barca Sánchez[8], D. Cebra[8], I. Chakaberia[31,6], P. Chaloupka[14], B. K. Chan[9], F-H. Chang[37], Z. Chang[6], N. Chankova-Bunzarova[28], A. Chatterjee[11], S. Chattopadhyay[61], D. Chen[10], J. Chen[49], J. H. Chen[18], X. Chen[48], Z. Chen[49], J. Cheng[57], M. Chevalier[10], S. Choudhury[18], W. Christie[6], X. Chu[6], H. J. Crawford[7], M. Csanád[16], M. Daugherity[1], T. G. Dedovich[28], I. M. Deppner[19], A. A. Derevschikov[43], A. Dhamija[41], L. Di Carlo[63], L. Didenko[6], P. Dixit[22], X. Dong[31], J. L. Drachenberg[1], E. Duckworth[29], J. C. Dunlop[6], N. Elsey[63], J. Engelage[7], G. Eppley[45], S. Esumi[58], O. Evdokimov[12], A. Ewigleben[32], O. Eyser[6], R. Fatemi[30], F. M. Fawzi[5], S. Fazio[6], P. Federic[38], J. Fedorisin[28], C. J. Feng[37], Y. Feng[44], P. Filip[28], E. Finch[51], Y. Fisyak[6], A. Francisco[64], C. Fu[11], L. Fulek[2], C. A. Gagliardi[55], T. Galatyuk[15], F. Geurts[45], N. Ghimire[54], A. Gibson[60], K. Gopal[23], X. Gou[49], D. Grosnick[60], A. Gupta[27], W. Guryn[6], A. I. Hamad[29], A. Hamed[5], Y. Han[45], S. Harabasz[15], M. D. Harasty[8], J. W. Harris[64], H. Harrison[30], S. He[11], W. He[18], X. H. He[26], Y. He[49], S. Heppelmann[8], S. Heppelmann[42], N. Herrmann[19], E. Hoffman[20], L. Holub[14], Y. Hu[18], H. Huang[37], H. Z. Huang[9], S. L. Huang[52], T. Huang[37], X. Huang[57], Y. Huang[57], T. J. Humanic[39], G. Igo[9,*], D. Isenhower[1], W. W. Jacobs[25], C. Jena[23], A. Jentsch[6], Y. Ji[31], J. Jia[6,52], K. Jiang[48], X. Ju[48], E. G. Judd[7], S. Kabana[53], M. L. Kabir[10], S. Kagamaster[32], D. Kalinkin[25,6], K. Kang[57], D. Kapukchyan[10], K. Kauder[6], H. W. Ke[6], D. Keane[29], A. Kechechyan[28], M. Kelsey[63], Y. V. Khyzhniak[35], D. P. Kikoła[62], C. Kim[10], B. Kimelman[8], D. Kincses[16], I. Kisel[17], A. Kiselev[6], A. G. Knospe[32], H. S. Ko[31], L. Kochenda[35], L. K. Kosarzewski[14], L. Kramarik[14], P. Kravtsov[35], L. Kumar[41], S. Kumar[26], R. Kunnawalkam Elayavalli[64], J. H. Kwasizur[25], R. Lacey[52], S. Lan[11], J. M. Landgraf[6], J. Lauret[6], A. Lebedev[6], R. Lednicky[28,38], J. H. Lee[6], Y. H. Leung[31], N. Lewis[6], C. Li[49], C. Li[48], W. Li[45], X. Li[48], Y. Li[57], X. Liang[10], Y. Liang[29], R. Licenik[38], T. Lin[49], Y. Lin[11], M. A. Lisa[39], F. Liu[11], H. Liu[25], H. Liu[11], P. Liu[52], T. Liu[64], X. Liu[39], Y. Liu[55], Z. Liu[48], T. Ljubicic[6], W. J. Llope[63], R. S. Longacre[6], E. Loyd[10], N. S. Lukow[54], X. F. Luo[11], L. Ma[18], R. Ma[6], Y. G. Ma[18], N. Magdy[12], D. Mallick[36], S. Margetis[29], C. Markert[56], H. S. Matis[31], J. A. Mazer[46], N. G. Minaev[43], S. Mioduszewski[55], B. Mohanty[36], M. M. Mondal[52], I. Mooney[63], D. A. Morozov[43], A. Mukherjee[16], M. Nagy[16], J. D. Nam[54], Md. Nasim[22], K. Nayak[11], D. Neff[9], J. M. Nelson[7], D. B. Nemes[64], M. Nie[49], G. Nigmatkulov[35], T. Niida[58], R. Nishitani[58], L. V. Nogach[43], T. Nonaka[58], A. S. Nunes[6], G. Odyniec[31], A. Ogawa[6], S. Oh[31], V. A. Okorokov[35], B. S. Page[6], R. Pak[6], J. Pan[55], A. Pandav[36], A. K. Pandey[58], Y. Panebratsev[28], P. Parfenov[35], B. Pawlik[40], D. Pawlowska[62], C. Perkins[7], L. Pinsky[20], J. Pluta[62], B. R. Pokhrel[54], G. Ponimatkin[38], J. Porter[31], M. Posik[54], V. Prozorova[14], N. K. Pruthi[41], M. Przybycien[2], J. Putschke[63], H. Qiu[26], A. Quintero[54], C. Racz[10], S. K. Radhakrishnan[29], N. Raha[63], R. L. Ray[56], R. Reed[32], H. G. Ritter[31], M. Robotkova[38], O. V. Rogachevskiy[28], J. L. Romero[8], D. Roy[46], L. Ruan[6], J. Rusnak[38], A. K. Sahoo[22], N. R. Sahoo[49], H. Sako[58], S. Salur[46], J. Sandweiss[64,*], S. Sato[58], W. B. Schmidke[6], N. Schmitz[33], B. R. Schweid[52], F. Seck[15], J. Seger[13], M. Sergeeva[9], R. Seto[10], P. Seyboth[33], N. Shah[24], E. Shahaliev[28], P. V. Shanmuganathan[6], M. Shao[48], T. Shao[18], A. I. Sheikh[29], D. Y. Shen[18], S. S. Shi[11], Y. Shi[49], Q. Y. Shou[18], E. P. Sichtermann[31], R. Sikora[2], M. Simko[38], J. Singh[41], S. Singha[26], M. J. Skoby[44], N. Smirnov[64], Y. Söhngen[19], W. Solyst[25], Y. Song[64], P. Sorensen[6], H. M. Spinka[4,*], B. Srivastava[44], T. D. S. Stanislaus[60], M. Stefaniak[62], D. J. Stewart[64], M. Strikhanov[35], B. Stringfellow[44], A. A. P. Suaide[47], M. Sumbera[38], B. Summa[42], X. M. Sun[11], X. Sun[12], Y. Sun[48], Y. Sun[21], B. Surrow[54], D. N. Svirida[3], Z. W. Sweger[8], P. Szymanski[62], A. H. Tang[6], Z. Tang[48], A. Taranenko[35], T. Tarnowsky[34], J. H. Thomas[31], A. R. Timmins[20], D. Tlusty[13], T. Todoroki[58], M. Tokarev[28], C. A. Tomkiel[32], S. Trentalange[9], R. E. Tribble[55], P. Tribedy[6], S. K. Tripathy[16], T. Truhlar[14], B. A. Trzeciak[14], O. D. Tsai[9], Z. Tu[6], T. Ullrich[6], D. G. Underwood[4,60], I. Upsal[45], G. Van Buren[6], J. Vanek[38], A. N. Vasiliev[43], I. Vassiliev[17], V. Verkest[63], F. Videbæk[6], S. Vokal[28], S. A. Voloshin[63], F. Wang[44], G. Wang[9], J. S. Wang[21], P. Wang[48], X. Wang[49], Y. Wang[11], Y. Wang[57], Z. Wang[49], J. C. Webb[6], P. C. Weidenkaff[19], L. Wen[9], G. D. Westfall[34], H. Wieman[31], S. W. Wissink[25], R. Witt[59], J. Wu[11], J. Wu[26], Y. Wu[10], B. Xi[50], Z. G. Xiao[57], G. Xie[31], W. Xie[44], H. Xu[21], N. Xu[31], Q. H. Xu[49], Y. Xu[49], Z. Xu[6], Z. Xu[9], G. Yan[49], C. Yang[49],

Q. Yang[49], S. Yang[45], Y. Yang[37], Z. Ye[45], Z. Ye[12], L. Yi[49], K. Yip[6], Y. Yu[49], H. Zbroszczyk[62], W. Zha[48], C. Zhang[52], D. Zhang[11], J. Zhang[49], S. Zhang[12], S. Zhang[18], X. P. Zhang[57], Y. Zhang[26], Y. Zhang[48], Y. Zhang[11], Z. J. Zhang[37], Z. Zhang[6], Z. Zhang[12], J. Zhao[44], C. Zhou[18], Y. Zhou[11], X. Zhu[57], M. Zurek[4], M. Zyzak[17]

(STAR Collaboration)

[1]Abilene Christian University, Abilene, Texas 79699
[2]AGH University of Science and Technology, FPACS, Cracow 30-059, Poland
[3]Alikhanov Institute for Theoretical and Experimental Physics NRC "Kurchatov Institute", Moscow 117218, Russia
[4]Argonne National Laboratory, Argonne, Illinois 60439
[5]American University of Cairo, New Cairo 11835, New Cairo, Egypt
[6]Brookhaven National Laboratory, Upton, New York 11973
[7]University of California, Berkeley, California 94720
[8]University of California, Davis, California 95616
[9]University of California, Los Angeles, California 90095
[10]University of California, Riverside, California 92521
[11]Central China Normal University, Wuhan, Hubei 430079
[12]University of Illinois at Chicago, Chicago, Illinois 60607
[13]Creighton University, Omaha, Nebraska 68178
[14]Czech Technical University in Prague, FNSPE, Prague 115 19, Czech Republic
[15]Technische Universität Darmstadt, Darmstadt 64289, Germany
[16]ELTE Eötvös Loránd University, Budapest, Hungary H-1117
[17]Frankfurt Institute for Advanced Studies FIAS, Frankfurt 60438, Germany
[18]Fudan University, Shanghai, 200433
[19]University of Heidelberg, Heidelberg 69120, Germany
[20]University of Houston, Houston, Texas 77204
[21]Huzhou University, Huzhou, Zhejiang 313000
[22]Indian Institute of Science Education and Research (IISER), Berhampur 760010 , India
[23]Indian Institute of Science Education and Research (IISER) Tirupati, Tirupati 517507, India
[24]Indian Institute Technology, Patna, Bihar 801106, India
[25]Indiana University, Bloomington, Indiana 47408
[26]Institute of Modern Physics, Chinese Academy of Sciences, Lanzhou, Gansu 730000
[27]University of Jammu, Jammu 180001, India
[28]Joint Institute for Nuclear Research, Dubna 141 980, Russia
[29]Kent State University, Kent, Ohio 44242
[30]University of Kentucky, Lexington, Kentucky 40506-0055
[31]Lawrence Berkeley National Laboratory, Berkeley, California 94720
[32]Lehigh University, Bethlehem, Pennsylvania 18015
[33]Max-Planck-Institut für Physik, Munich 80805, Germany
[34]Michigan State University, East Lansing, Michigan 48824
[35]National Research Nuclear University MEPhI, Moscow 115409, Russia
[36]National Institute of Science Education and Research, HBNI, Jatni 752050, India
[37]National Cheng Kung University, Tainan 70101
[38]Nuclear Physics Institute of the CAS, Rez 250 68, Czech Republic
[39]Ohio State University, Columbus, Ohio 43210
[40]Institute of Nuclear Physics PAN, Cracow 31-342, Poland
[41]Panjab University, Chandigarh 160014, India
[42]Pennsylvania State University, University Park, Pennsylvania 16802
[43]NRC "Kurchatov Institute", Institute of High Energy Physics, Protvino 142281, Russia
[44]Purdue University, West Lafayette, Indiana 47907
[45]Rice University, Houston, Texas 77251
[46]Rutgers University, Piscataway, New Jersey 08854
[47]Universidade de São Paulo, São Paulo, Brazil 05314-970
[48]University of Science and Technology of China, Hefei, Anhui 230026
[49]Shandong University, Qingdao, Shandong 266237
[50]Shanghai Institute of Applied Physics, Chinese Academy of Sciences, Shanghai 201800
[51]Southern Connecticut State University, New Haven, Connecticut 06515
[52]State University of New York, Stony Brook, New York 11794
[53]Instituto de Alta Investigación, Universidad de Tarapacá, Arica 1000000, Chile
[54]Temple University, Philadelphia, Pennsylvania 19122
[55]Texas A&M University, College Station, Texas 77843
[56]University of Texas, Austin, Texas 78712
[57]Tsinghua University, Beijing 100084
[58]University of Tsukuba, Tsukuba, Ibaraki 305-8571, Japan
[59]United States Naval Academy, Annapolis, Maryland 21402

[60]Valparaiso University, Valparaiso, Indiana 46383

[61]Variable Energy Cyclotron Centre, Kolkata 700064, India

[62]Warsaw University of Technology, Warsaw 00-661, Poland

[63]Wayne State University, Detroit, Michigan 48201

[64]Yale University, New Haven, Connecticut 06520 and

*Deceased

(Dated: December 2, 2021)

We report cumulants of the proton multiplicity distribution from dedicated fixed-target Au+Au collisions at $\sqrt{s_{\mathrm{NN}}} = 3.0$ GeV, measured by the STAR experiment in the kinematic acceptance of rapidity (y) and transverse momentum (p_{T}) within $-0.5 < y < 0$ and $0.4 < p_{\mathrm{T}} < 2.0$ GeV/c. In the most central 0–5% collisions, a proton cumulant ratio is measured to be $C_4/C_2 = -0.85 \pm 0.09$ (stat.)± 0.82 (syst.), which is less than unity, the Poisson baseline. The hadronic transport UrQMD model reproduces our C_4/C_2 in the measured acceptance. Compared to higher energy results and the transport model calculations, the suppression in C_4/C_2 is consistent with fluctuations driven by baryon number conservation and indicates an energy regime dominated by hadronic interactions. These data imply that the QCD critical region, if created in heavy-ion collisions, could only exist at energies higher than 3 GeV.

With the discovery of the quark-gluon plasma (QGP) at the Relativistic Heavy Ion Collider (RHIC) [1–4], physicists are starting to investigate the phase structure of the QCD matter, especially in the high baryon density region. The stark differences between the properties of QGP and lower energy nuclear matter draw interest to the thermodynamic processes, specifically those related to the nature of phase transitions [5]. Experimenters can access the QCD phase diagram, expressed in temperature (T) and baryonic chemical potential (μ_B), and search for phase boundaries by varying the heavy-ion collision energy. At regions of equal baryon and anti-baryon density, $\mu_B = 0$, theoretical approaches work well, with lattice QCD calculations predicting a smooth cross-over transition from hadronic matter to a QGP [6, 7]. At finite μ_B, where the baryon density is larger than the anti-baryon density, the existence and nature of the phase transition are not well understood.

The event-by-event fluctuations of conserved quantities such as net charge, net-baryon number, and net strangeness are predicted to depend on the non-equilibrium correlation length, ξ, and thus serve as indicators of critical behavior [8]. Ideally, near the singular critical point, the correlation length could grow as large as the size of the system under study, provided sufficient time for the development. In heavy-ion collisions, however, effects from the finite size and limited lifetime of the hot nuclear system will limit the significance of signals [9]. A theoretical calculation suggests that ξ may rise from ~ 0.5 to 3 fm in heavy-ion collisions, constrained by the size of the system [10]. Experimentally, protons and anti-protons are measured with high efficiency [11] and have been shown to be reliable proxies for baryons and anti-baryons [8]. Despite computational challenges at finite μ_B [12, 13], lattice QCD calculations have predicted a positive cumulant ratio of net-proton (proton minus anti-proton) C_4/C_2 for the formation of QGP matter at finite μ_B.

Recent reports on net-proton fluctuation measurements from RHIC's first phase of the Beam Energy Scan program (BES-I) [14, 15] have demonstrated the potential sensitivity of the cumulant ratios of C_3/C_2 and C_4/C_2 of the net-proton multiplicity distribution to the collision energy. Due to baryon number conservation, calculations from both hadron resonance gas models (HRG) of the canonical ensemble [16, 17] and the Ultrarelativistic Quantum Molecular Dynamics (UrQMD) [17] transport model, which do not contain critical dynamics, produce a smooth energy dependence. Above a center of mass energy ($\sqrt{s_{\mathrm{NN}}}$) of 27 GeV, the Solenoidal Tracker at RHIC (STAR) collaboration's BES-I results agree well with the HRG and UrQMD models [14, 15]. However, in the energy range $7.7 < \sqrt{s_{\mathrm{NN}}} < 27$ GeV from the top 5% central Au+Au collisions at RHIC, STAR's results show a non-monotonic behavior as a function of $\sqrt{s_{\mathrm{NN}}}$ with a significance of 3.1σ [14, 15]. Here, the centrality is a measure of the geometric overlap of two colliding nuclei and is defined by a charged particle multiplicity. At collision energies below $\sqrt{s_{\mathrm{NN}}} = 7.7$ GeV, where net baryon densities are high, UrQMD predicts a suppression with respect to unity of C_4/C_2 for central events. For all energies, a gas of classical free particles (Poisson distribution) has a C_4/C_2 of 1. A remaining question is how the non-monotonic behavior continues in a higher baryon density region below $\sqrt{s_{\mathrm{NN}}} = 7.7$ GeV.

In this paper, we report the cumulant ratios of proton multiplicity distributions in Au+Au collisions at $\sqrt{s_{\mathrm{NN}}} = 3.0$ GeV. For the top 5% central collisions, the dependence of cumulant ratios on the particle rapidity (y) and transverse momentum (p_{T}) is presented along with comparisons to model calculations. At this energy, the anti-proton production is negligible ($\overline{p}/p \sim \exp(-2\mu_B/T_{\mathrm{ch}}) < 10^{-6}$) [18], therefore only the proton multiplicity distribution is used in the analysis.

The AGS-RHIC accelerator complex provided a gold beam with an energy of 3.85 GeV, incident on a gold target, corresponding to $\sqrt{s_{\mathrm{NN}}} = 3.0$ GeV for Au+Au fixed-target collisions. At this energy, STAR's fixed-target

mode (FXT) [19, 20] covered the mid-rapidity for protons in the center-of-mass frame. The proton multiplicities are determined using the Time Projection Chamber (TPC) and Time of Flight detector (TOF) of the STAR [21]. The target was located 200.7 cm from the center of the TPC and of thickness 1.93 g/cm^2 (0.25 mm) corresponding to a 1% interaction probability. The TPC measures both the trajectory and the energy loss (dE/dx) of a particle. The TPC is placed within a solenoidal magnetic field (0.5 Tesla) and the particle momenta are calculated from their curvatures. For these data, RHIC was configured to circulate twelve bunches of 7×10^9 gold ions, which grazed the top of the gold target. To remove collisions between the beam and the beam pipe, event vertices are required to be less than 1.3 cm from the Au target along the beam line and less than 1.5 cm from the target radially from the mean collision vertex. The analysis is performed with 1.4×10^8 events.

The collisions are characterized by their centrality, inferred from reconstructed particle multiplicities (reference multiplicity). For this analysis, the reference multiplicity is the total number of tracks in the TPC uncorrected for efficiency loss, excluding baryons via dE/dx. The TPC covered all azimuthal angles and the pseudorapidity η of $0 < \eta < 2$, in which $\eta \equiv -\ln[\tan(\theta/2)]$ and θ is the angle between the particle three-momentum and the beam axis in the lab frame. Proton tracks are excluded from the reference multiplicity to avoid self-correlations [14, 15, 22]. The reference multiplicity distribution shown in Fig. 1 is fit with a Monte Carlo Glauber model (GM) coupled with a two component particle production model [23, 24]. By integrating the GM fit, events are categorized into seven centrality classes: 0–5, 5–10, 10–20, ..., 50–60%. At reference multiplicities below 10, the experimental data and the GM disagree due to inefficiency in the experimental trigger system. At multiplicities above 80, double collision (pile-up) events dominate the multiplicity distribution. In addition to a pile-up correction discussed below, events above the reference multiplicity of 80 are removed from the 0–5% centrality class.

In the FXT collisions, due to finite target thickness, the pile-up is clearly present, see Fig. 1. The cumulants are corrected for the effect of pile-up using an unfolding method [25, 26]. As a result, the single and double collisions are separated statistically. Figure 1 shows the input GM fit (red curve) and the unfolded pile-up distribution (green dashed curve). The single collision distribution is extracted (blue points) from the measured distribution (black dots) and the unfolded pile-up distribution. The event-averaged pile-up probability, or total pile-up fraction, is determined to be $(0.46 \pm 0.09)\%$ of all events and $(2.10 \pm 0.40)\%$ in the 0–5% centrality class.

Figure 2(a) shows dE/dx versus the particle rigidity for all positively charged tracks in the STAR TPC. The pion, kaon, proton, and deuteron bands are labeled and a theo-
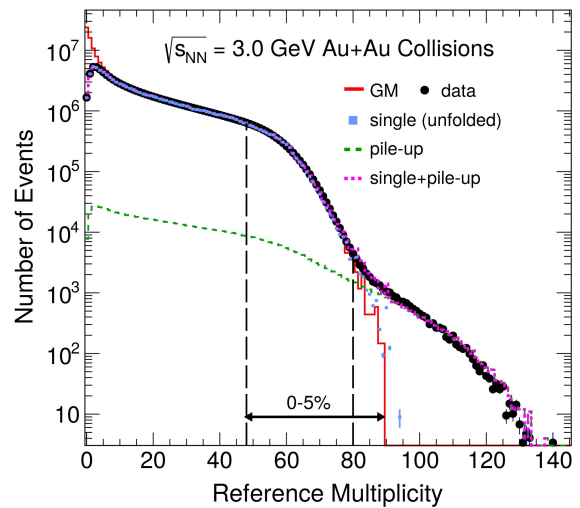

FIG. 1. Reference multiplicity distributions obtained from $\sqrt{s_{\mathrm{NN}}} = 3.0$ GeV data (black markers), GM (red histogram), and single and pile-up contributions from unfolding. Vertical lines on markers represent statistical uncertainties. Single, pile-up and single+pile-up collisions are shown in solid blue markers, dashed green and dashed magenta curves, respectively. Analysis is performed on 0–5% central events, indicated by a black arrow.

retical prediction [27] for the proton energy loss is shown in red. Below rigidities of 2.0 GeV/c, the proton dE/dx band is well separated and the TPC provides sufficient particle identification. To improve the particle identification for tracks with momenta above 2.0 GeV/c, TPC tracks are matched with TOF hits and a mass-squared cut of $0.6 < m^2 < 1.2$ (GeV/c^2)^2 is placed. The TOF requirement introduces a 60% matching efficiency. The proton purity is required to be higher than 95% at all rapidities and momenta for the subsequent cumulant analysis.

Figure 2(b) displays the $p_{\mathrm{T}}-y$ acceptance in the center-of-mass frame for protons in fixed-target collisions at $\sqrt{s_{\mathrm{NN}}} = 3.0$ GeV. The black box in Fig. 2(b) indicates the acceptance window ($-0.5 < y < 0$, $0.4 < p_{\mathrm{T}} < 2.0$ GeV/c) used. The red dashed box shows the maximum symmetric rapidity window ($|y| < 0.1$) for the selected p_{T} region ($0.4 < p_{\mathrm{T}} < 2.0$ GeV/c). The target, depicted by a black arrow, is at rapidity $y = -1.05$. The diagonal discontinuity in Fig. 2(b) is caused by the mass-squared cut above total momenta of 2.0 GeV/c in the lab frame. The vertical line structure above 2.0 GeV/c, most prominent within $-1.0 < y < -0.2$, results from the geometry of the TOF modules.

Experimentally measured proton multiplicity distributions are described by the central moments, i.e., $\langle (\delta N)^2 \rangle$, $\langle (\delta N)^3 \rangle$ and so on. The symbol $\langle ... \rangle$ indicates the average over all the events, N is the proton multiplicity in a given event, and $\delta N = N - \langle N \rangle$ is the deviation. The relations
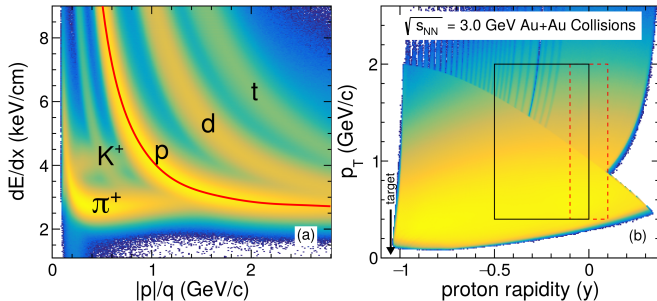
FIG. 2. Left panel (a): dE/dx versus particle rigidity measured in the TPC; pion, kaon, proton, deuteron, and triton bands are labeled. The theory prediction for protons is plotted in red. The electron peak is in between the pion and kaon bands. Right panel (b): Analysis acceptance in transverse momentum versus proton rapidity (y) in the center-of-mass frame of Au+Au collisions at $\sqrt{s_{NN}} = 3.0$ GeV. The black box indicates the acceptance within $-0.5 < y < 0$ and $0.4 < p_T < 2.0$ GeV/c. The red dashed box indicates a narrower rapidity window $|y| < 0.1$, the largest possible symmetric rapidity window from this data set. In both panels, the yellow-to-blue color scale indicates the intensity.

between the cumulants C_n and the central moments are defined as:

$$
\begin{aligned}
\text{mean}: \mathrm{M} &= \langle N \rangle &&= C_1, \\
\text{variance}: \sigma^2 &= \langle (\delta N)^2 \rangle &&= C_2, \\
\text{skewness}: \mathrm{S} &= \langle (\delta N)^3 \rangle / \sigma^3 &&= C_3/C_2^{3/2}, \\
\text{kurtosis}: \kappa &= \langle (\delta N)^4 \rangle / \sigma^4 - 3 &&= C_4/C_2^2.
\end{aligned}
\tag{1}
$$

Ratios of the cumulants are often used to reduce volume dependence: $C_2/C_1 = \sigma^2/M$, $C_3/C_2 = S\sigma$, and $C_4/C_2 = \kappa\sigma^2$. An additional advantage is that the ratios of these cumulants can be readily compared with theoretical calculations of susceptibility [28–34] ratios $\sigma^2/M = \chi_2/\chi_1$, $S\sigma = \chi_3/\chi_2$, and $\kappa\sigma^2 = \chi_4/\chi_2$.

The proton cumulants and ratios are corrected for detector inefficiency and background from pile-up collisions. The potential background from spallation in the beam pipe is reduced by the lower transverse momentum cut $(p_T > 0.4$ GeV/$c)$. Detector efficiency corrections are performed on a "track-by-track" basis [35, 36], where the proton reconstruction efficiency as a function of p_T and rapidity is applied as a weight to each track. The integrated proton track efficiency for the TPC detector is 95% in the selected kinematic windows and centrality class (0–5%).

All cumulant ratios are compared to the Poisson baseline for which cumulants of all orders are the same $C_n=M$ and the cumulant ratios are equal to one. To suppress the spectator protons from entering the analysis, the maximum rapidity range is restricted to $-0.5 < y < 0$. For the rapidity dependence measurement $(y_{\min} < y < 0)$, the minimum rapidity $(y_{\min})$ is varied from -0.5 to -0.2

within $0.4 < p_T < 2.0$ GeV/c. For the transverse momentum dependence $(0.4 < p_T < p_T^{\max})$, $p_T^{\max}$ is varied from 0.8 to 2.0 GeV/c within $-0.5 < y < 0$. The proton cumulants C_1 through C_4 are provided in the supplemental material [37].

The statistical uncertainties are obtained using a Bootstrap approach [38, 39]. They are smaller than the marker size in the following figures. The systematic uncertainties are calculated from the uncertainty associated with the detector efficiency, the track selection criteria, and the pile-up correction. To estimate the uncertainties in the track selection criteria, the mass-squared window, the number of TPC space points required, and the distance of closest approach (DCA) in 3-dimensions of the reconstructed track's trajectory to the primary vertex position was varied. The DCA was varied from 1–3 cm. The analysis used a DCA < 3 cm cut. The uncertainty in the pile-up correction method is estimated by varying the pile-up fraction by its statistical uncertainty. For the top 5% central collisions, the largest contributions to the systematic uncertainty for C_4/C_2 are from the pile-up correction (± 0.24) and the DCA variation (± 0.78).

In a heavy-ion collision, the presence of non-critical fluctuations of the collision volume, [40] also known as volume fluctuations (VF), may lead to an artificial enhancement in the measured cumulants [38, 41]. As mentioned earlier, the information of collision centrality, expressed either in the fraction of total interaction cross section or in the averaged number of participating nucleons $\langle N_{part} \rangle$, is extracted from the measured charged particle multiplicity distributions, see Fig. 1. To achieve results properly weighted by the event statistics, a centrality bin width correction (CBWC) [15] is applied to all cumulants data discussed below. In comparison to BES-I, however, the centrality resolution in Au+Au collisions at $\sqrt{s_{NN}} = 3.0$ GeV is lower due to a decrease in the particle multiplicity. Therefore, volume fluctuation corrections (VFC) [40, 42] are tested with both the hadronic transport model UrQMD [17] and Glauber model [23].

Figure 3 depicts the cumulant ratios as a function of the average number of participating nucleons $\langle N_{part} \rangle$. The data with VFC, using N_{part} distributions extracted from UrQMD and Glauber models, and without VFC are shown as triangles, circles, and open squares, respectively. It is clear that the volume fluctuation correction shows a strong model dependence and affects the distribution, particularly in peripheral collisions. The respective dynamics in the UrQMD and Glauber model for charged hadron production lead to two different mappings from the measured final charged hadron multiplicity distributions to the initial geometry. This difference is likely the dominant source of the model dependence in the VFC. On the other hand, one can see in the figure that the difference between results with and without the VFC is small for higher order ratios C_3/C_2 and C_4/C_2 in the most central bin. As discussed in Refs. [43, 44], the

maximum number of participants, $N_{\text{part}}^{\max}$ (394 for Au+Au collisions), suppresses the initial volume fluctuations.
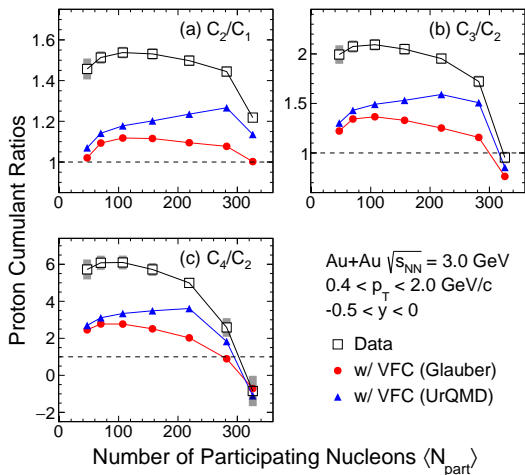

FIG. 3. Centrality dependence of the proton cumulant ratios for Au+Au collisions at $\sqrt{s_{\text{NN}}} = 3.0$ GeV. Protons are from $-0.5 < y < 0$ and $0.4 < p_{\text{T}} < 2.0$ GeV/c. Systematic uncertainties are represented by gray bars. Statistical uncertainties are smaller than marker size. CBWC is applied to all cumulant ratios. While open squares represent the data without correction, blue triangles and red circles are the results with VFC using the $\langle N_{\text{part}} \rangle$ distributions from the UrQMD and Glauber models, respectively.
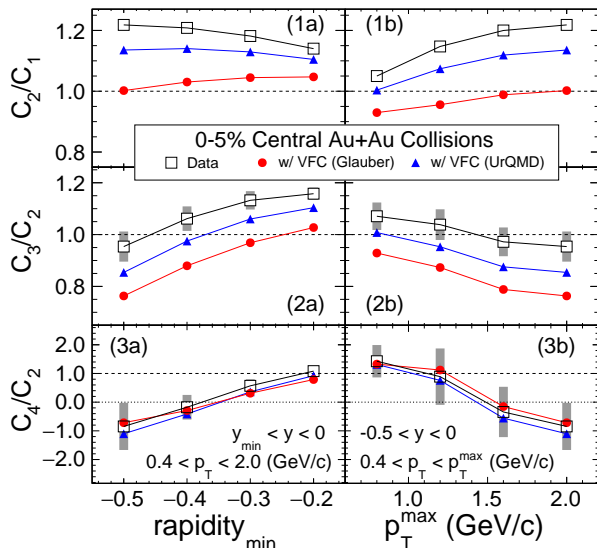
FIG. 4. Similar to Fig. 3: Rapidity and transverse momentum dependence of the proton cumulant ratios for 0–5% central collisions. Black-squares, red-dots and blue-triangles stand for data without and with the VFC using Glauber and UrQMD, respectively.

Figure 4 depicts the cumulant ratios as a function of rapidity y and transverse momentum p_{T} in 0–5% central collisions without and with the VFC. It is expected [45–

47] that the cumulant ratios approach the Poisson baseline in the limit of small acceptance. For C_3/C_2, the ratios with the VFC (UrQMD) and without the VFC deviate from the Poisson baseline at the narrow rapidity windows. The VFC (Glauber) ratio approaches unity as the acceptance is decreased. For the C_4/C_2 ratio, the VFC has a negligible effect in the most central bin. Therefore, C_4/C_2 is reported without VFC in the discussions below. In the central 0–5% collisions, as shown in Fig. 4, one obtains $C_4/C_2 = -0.85 \pm 0.09$ (stat.) ± 0.82 (syst.) in the kinematic acceptance of $-0.5 < y < 0$ and $0.4 < p_{\text{T}} < 2.0$ GeV/c. The UrQMD model qualitatively reproduces the acceptance dependence of the data, see Fig. 6 in the supplemental material [37].
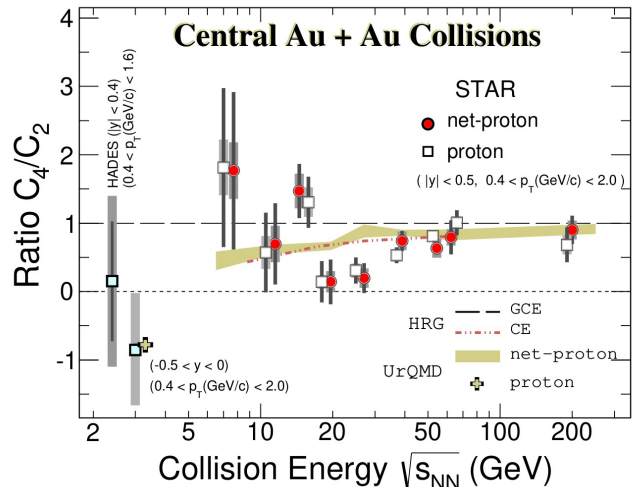

FIG. 5. Collision energy dependence of the ratios of cumulants, C_4/C_2, for proton (squares) and net-proton (red circles) from top 0–5% Au+Au collisions at RHIC [14, 15]. The points for protons are shifted horizontally for clarity. The new result for proton from $\sqrt{s_{\text{NN}}} = 3.0$ GeV collisions is shown as a filled square. HADES data of $\sqrt{s_{\text{NN}}} = 2.4$ GeV 0–10% collisions [48] is also shown. The vertical black and gray bars are the statistical and systematic uncertainties, respectively. In addition, results from the HRG model, based on both Canonical Ensemble (CE) and Grand-Canonical Ensemble (GCE), and transport model UrQMD are presented.

A non-monotonic energy dependence of the net-proton C_4/C_2 was reported for 0–5% central Au+Au collisions at $\sqrt{s_{\text{NN}}} = 7.7$–200 GeV [14, 15]. A similar energy dependence of the C_4/C_2 of protons is also evident (open squares in Fig. 5). Though a minimum appears around 20 GeV, both the C_4/C_2 ratio of protons and net-protons at 7.7 GeV are close to unity, albeit the large statistical uncertainties. Meanwhile, the C_4/C_2 value for Au+Au collisions at $\sqrt{s_{\text{NN}}} = 3.0$ GeV is around -1. The negative value of the proton C_4/C_2 is reasonably reproduced by the transport model UrQMD [17, 49].

The study of cumulant ratios in heavy-ion collisions has motivated several QCD inspired model cal-

culations [5], which report a similar oscillation pattern around the critical point due to the symmetry of the medium [50–55]. However, due to the stochastic nature of heavy-ion collisions, the finite lifetime and size of the system [56], and dynamical effects such as the critical slowing will smear the "critical point" to a region in collision energy [57, 58].

Poisson statistics and the Grand Canonical Ensemble (GCE) model predict that C_4/C_2 is 1. Because of baryon number conservation, calculations from models without critical dynamics such as the Canonical Ensemble (CE) [16] and UrQMD [49] show a characteristic suppression with respect to the Poisson baseline in the net-proton C_4/C_2 when the collision energy is decreased, as seen in Fig. 5. The same experimental cuts on event centrality, rapidity, and transverse momentum have been applied to these calculations. It is worth noting that if the rapidity window is extended to $|y| < 0.5$, the UrQMD model predicts a value of $C_4/C_2 \approx -4$ for proton in central Au+Au collisions at $\sqrt{s_{\rm NN}} = 3.0$ GeV. Compared to results from higher energy collisions, the suppression of the C_4/C_2 ratio in central Au+Au collisions at 3.0 GeV is stronger due to baryon stopping and conservation. Recently, a hadronic equation of state for 3.0 GeV Au+Au collisions was shown to be applicable, using the measurement of collective flow parameters [59]. While the low C_4/C_2 value observed at the energy can be explained by fluctuations driven by baryon number conservation in a region of high baryon density where hadronic interactions are dominant, the non-monotonic variation [14, 15] observed at higher collision energies is not demonstrated by the dynamics in non-critical models such as UrQMD. Precision data from the energy window of $3 < \sqrt{s_{\rm NN}} < 20$ GeV are needed in order to explore the possibility of critical phenomena.

In summary, cumulant ratios of proton multiplicity distribution from $\sqrt{s_{\rm NN}} = 3.0$ GeV Au+Au collisions are reported. The new data are measured by the STAR experiment configured in fixed-target mode. At this collision energy, large effects due to the initial volume fluctuation are observed in the cumulant ratios except in the most central 0–5% bin. The protons are measured with the acceptance $-0.5 < y < 0$ and $0.4 < p_{\rm T} < 2.0$ GeV/c. The rapidity and transverse momentum dependencies of the cumulant ratios C_2/C_1, C_3/C_2, and C_4/C_2 are presented. A suppression with respect to the Poisson baseline is observed in proton $C_4/C_2 = -0.85 \pm 0.09$ (stat) ± 0.82 (syst) in the most central 0–5% collisions at 3 GeV and the UrQMD model reproduces the data. Recall, Lattice QCD calculations predict a positive C_4/C_2 ratio for the formation of QGP matter [13, 60] at vanishing net baryon density. This new result is consistent with fluctuations driven by baryon number conservation at the high baryon density region.

[1] I. Arsene *et al.* (BRAHMS), Nucl. Phys. A **757**, 1 (2005), arXiv:nucl-ex/0410020.

[2] B. B. Back *et al.* (PHOBOS), Nucl. Phys. A **757**, 28 (2005), arXiv:nucl-ex/0410022.

[3] K. Adcox *et al.* (PHENIX), Nucl. Phys. A **757**, 184 (2005), arXiv:nucl-ex/0410003.

[4] J. Adams *et al.* (STAR), Nucl. Phys. A **757**, 102 (2005), arXiv:nucl-ex/0501009.

[5] M. A. Stephanov, Phys. Rev. Lett. **107**, 052301 (2011), arXiv:1104.1627 [hep-ph].

[6] S. Borsanyi *et al.*, Phys. Lett. B **730**, 99 (2014), arXiv:1309.5258 [hep-lat].

[7] S. Gupta, X. Luo, B. Mohanty, H. G. Ritter, and N. Xu, Science **332**, 1525 (2011), arXiv:1105.3934 [hep-ph].

[8] Y. Hatta and M. A. Stephanov, Phys. Rev. Lett. **91**, 102003 (2003).

[9] E. S. Fraga, T. Kodama, L. F. Palhares, and P. Sorensen, PoS FACESQCD **117**, 017 (2010), arXiv:1106.3887 [hep-ph].

[10] B. Berdnikov and K. Rajagopal, Phys. Rev. D **61**, 105017 (2000), arXiv:hep-ph/9912274.

[11] M. M. Aggarwal *et al.* (STAR), Phys. Rev. Lett. **105**, 022302 (2010), arXiv:1004.4959 [nucl-ex].

[12] A. Bazavov *et al.* (HotQCD), Phys. Rev. D **96**, 074510 (2017), arXiv:1708.04897 [hep-lat].

[13] R. Bellwied *et al.*, arXiv:2102.06625 [hep-lat].

[14] J. Adam *et al.* (STAR), Phys. Rev. Lett. **126**, 092301 (2021), arXiv:2001.02852 [nucl-ex].

[15] M. Abdallah *et al.* (STAR), Phys. Rev. C **104**, 024902 (2021), arXiv:2101.12413 [nucl-ex].

[16] P. Braun-Munzinger *et al.*, Nucl. Phys. A **1008**, 122141

(2021), arXiv:2007.02463 [nucl-th].

[17] S. A. Bass *et al.*, Prog. Part. Nucl. Phys. **41**, 255 (1998), arXiv:nucl-th/9803035.

[18] A. Andronic, P. Braun-Munzinger, K. Redlich, and J. Stachel, Nature **561**, 321 (2018), arXiv:1710.09425 [nucl-th].

[19] M. S. Abdallah *et al.* (STAR), arXiv:2108.00044 [nucl-ex] (2021).

[20] M. S. Abdallah *et al.* (STAR), Phys. Rev. C **103**, 034908 (2021), arXiv:2007.14005 [nucl-ex].

[21] W. J. Llope (STAR), Nucl. Instrum. Meth. A **661**, S110 (2012).

[22] A. Chatterjee *et al.*, Phys. Rev. C **101**, 034902 (2020), arXiv:1910.08004 [nucl-ex].

[23] M. L. Miller, K. Reygers, S. J. Sanders, and P. Steinberg, Ann. Rev. Nucl. Part. Sci. **57**, 205 (2007), arXiv:nucl-ex/0701025.

[24] B. I. Abelev *et al.* (STAR), Phys. Rev. C **81**, 024911 (2010), arXiv:0909.4131 [nucl-ex].

[25] T. Nonaka, M. Kitazawa, and S. Esumi, Nucl. Instrum. Meth. A **984**, 164632 (2020), arXiv:2006.15809 [physics.data-an].

[26] Y. Zhang, Y. Huang, T. Nonaka, and X. Luo, (2021), arXiv:2108.10134 [physics.data-an].

[27] H. Bichsel, Nucl. Instrum. Meth. A **562**, 154 (2006).

[28] S. Ejiri, F. Karsch, and K. Redlich, Phys. Lett. B **633**, 275 (2006).

[29] B. Friman, F. Karsch, K. Redlich, and V. Skokov, Eur. Phys. J. C **71**, 1694 (2011), arXiv:1103.3511 [hep-ph].

[30] F. Karsch and K. Redlich, Phys. Lett. B **695**, 136 (2011).

[31] A. Bazavov *et al.*, Phys. Rev. Lett. **109**, 192302 (2012).

[32] W. J. Fu, X. Luo, J. M. Pawlowski, F. Rennecke, R. Wen, and S. Yin, Phys. Rev. D **104**, 094047 (2021).

[33] S. Borsányi *et al.*, Phys. Rev. Lett. **111**, 062005 (2013).

[34] P. Alba *et al.*, Phys. Lett. B **738**, 305 (2014).

[35] T. Nonaka, M. Kitazawa, and S. Esumi, Phys. Rev. C **95**, 064912 (2017).

[36] X. Luo and T. Nonaka, Phys. Rev. C **99**, 044917 (2019), arXiv:1812.10303v2.

[37] See Supplemental Material at [link] for discussion of UrQMD model calculations, pile up correction method, volume fluctuation correction methods and symmetric rapidity measurement.

[38] X. Luo, J. Xu, B. Mohanty, and N. Xu, J. Phys. G **40**, 105104 (2013), arXiv:1302.2332 [nucl-ex].

[39] A. Pandav, D. Mallick, and B. Mohanty, Nucl. Phys. A **991**, 121608 (2019), arXiv:1809.08892 [nucl-ex].

[40] V. Skokov, B. Friman, and K. Redlich, Phys. Rev. C **88**, 034911 (2013), arXiv:1205.4756 [hep-ph].

[41] S. He and X. Luo, Chin. Phys. C **42**, 104001 (2018), arXiv:1802.02911 [physics.data-an].

[42] P. Braun-Munzinger, A. Rustamov, and J. Stachel, Nucl. Phys. A **960**, 114 (2017).

[43] M. Mackowiak-Pawlowska, M. Naskręt, and M. Gazdzicki, Nucl. Phys. A **1014**, 122258 (2021), arXiv:2102.11186 [hep-ex].

[44] H. Xu, Phys. Rev. C **94**, 054903 (2016), arXiv:1602.07089 [nucl-th].

[45] B. Ling and M. A. Stephanov, Phys. Rev. C **93**, 034915 (2016), arXiv:1512.09125 [nucl-th].

[46] A. Bzdak and V. Koch, Phys. Rev. C **96**, 054905 (2017), arXiv:1707.02640 [nucl-th].

[47] J. Brewer, S. Mukherjee, K. Rajagopal, and Y. Yin, Phys. Rev. C **98**, 061901 (2018), arXiv:1804.10215 [hep-ph].

[48] J. Adamczewski-Musch *et al.* (HADES), Phys. Rev. C **102**, 024914 (2020), arXiv:2002.08701 [nucl-ex].

[49] M. Bleicher *et al.*, J. Phys. G **25**, 1859 (1999), arXiv:hep-ph/9909407.

[50] B. J. Schaefer and M. Wagner, Phys. Rev. D **85**, 034027 (2012), arXiv:1111.6871 [hep-ph].

[51] J. W. Chen, J. Deng, H. Kohyama, and L. Labun, Phys. Rev. D **93**, 034037 (2016), arXiv:1509.04968 [hep-ph].

[52] W. J. Fu, J. M. Pawlowski, F. Rennecke, and B.-J. Schaefer, Phys. Rev. D **94**, 116020 (2016), arXiv:1608.04302 [hep-ph].

[53] G. Shao, Z. Tang, X. Gao, and W. He, Eur. Phys. J. C **78**, 138 (2018), arXiv:1708.04888 [hep-ph].

[54] Z. Li, K. Xu, X. Wang, and M. Huang, Eur. Phys. J. C **79**, 245 (2019), arXiv:1801.09215 [hep-ph].

[55] D. Mroczek *et al.*, Phys. Rev. C **103**, 034901 (2021), arXiv:2008.04022 [nucl-th].

[56] Y. Y. Wang *et al.*, Chin. Phys. C **35**, 264 (2011).

[57] J. Weil *et al.*, Phys. Rev. C **94**, 054905 (2016), arXiv:1606.06642 [nucl-th].

[58] C. Shen and L. Yan, Nucl. Sci. Tech. **31**, 122 (2020), arXiv:2010.12377 [nucl-th].

[59] M. Abdallah *et al.* (STAR), arXiv:2108.00908 [nucl-ex] (2021).

[60] A. Bazavov *et al.*, Phys. Rev. D **101**, 074502 (2020), arXiv:2001.08530 [hep-lat].

SUPPLEMENTAL MATERIAL

(Dated: December 2, 2021)

I. URQMD MODEL CALCULATION

This paper includes a comparison of the proton multiplicity distributions from the experimental data and the UrQMD model [1, 2] for Au+Au collisions at $\sqrt{s_{\mathrm{NN}}} = 3.0$ GeV. The UrQMD model is a microscopic transport model that does not contain critical phenomena physics. The sample is produced using UrQMD version 3.4 in cascade mode and consists of ∼80 million events. The kinematic cuts used in the UrQMD calculation and the data analysis are the same ($-0.5 < y < 0$ and $0.4 < p_{\mathrm{T}} < 2.0$ GeV/c). To determine centrality, similar techniques are applied to reference multiplicity distributions of both the data and UrQMD samples. The reference multiplicity of an event is defined as the charged particle multiplicity excluding protons. Figure 1 shows a comparison of the multiplicity distributions from the data and the UrQMD model. In addition, the UrQMD reference multiplicity distribution is scaled to match the $\sqrt{s_{\mathrm{NN}}} = 3.0$ GeV data. All statistical uncertainties in the UrQMD analysis are calculated using the Delta theorem [3, 4].
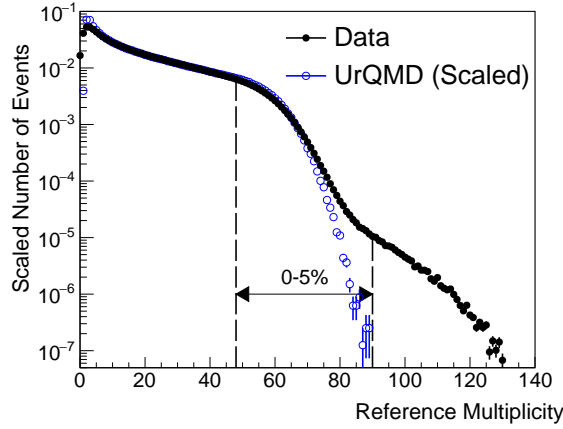

FIG. 1. Comparison of reference multiplicity distribution between data and UrQMD model for Au+Au collisions at $\sqrt{s_{\mathrm{NN}}} = 3.0$ GeV. Reference multiplicity is charged particle multiplicity without protons.

II. PILE-UP CORRECTION

In the fixed target run, the largest source of background was pile-up, which is defined as two or more collisions reconstructed as a single event. One can see the pile-up in the high tail (> 80) of reference multiplicity distribution (see Fig. 1). Using an analytical method [5], the measured cumulants are corrected for the effect of pile-up collisions. The method requires the event-averaged pile-up fraction at each multiplicity bin. Figure 2 shows proton cumulants and ratios up-to 4$^{\mathrm{th}}$-order. The star and circle markers represent data with and without the pile-up correction method applied, respectively. The most central collisions are most affected by the pile-up event contamination.

III. VOLUME FLUCTUATION CORRECTION

In heavy-ion collisions, the collision volume can be defined by the number of participating nucleons N_{part}. It cannot be directly measured but is inferred through the correlation or anti-correlation of a detector measurement. In this analysis, the cumulants are calculated at finite multiplicity bins which have an underlying N_{part} distribution. It has been shown [6] that the fluctuations of the N_{part} distribution can cause artificial enhancements in the measured cumulants. This enhancement is referred to as volume fluctuations (VF). In comparison to higher energy collisions, the overall particle production is lower in Au+Au collisions at $\sqrt{s_{\mathrm{NN}}} = 3.0$ GeV. Thus, the resolution of the reference multiplicity is lower, which decreases the centrality resolution and increases the effect from volume fluctuations. A
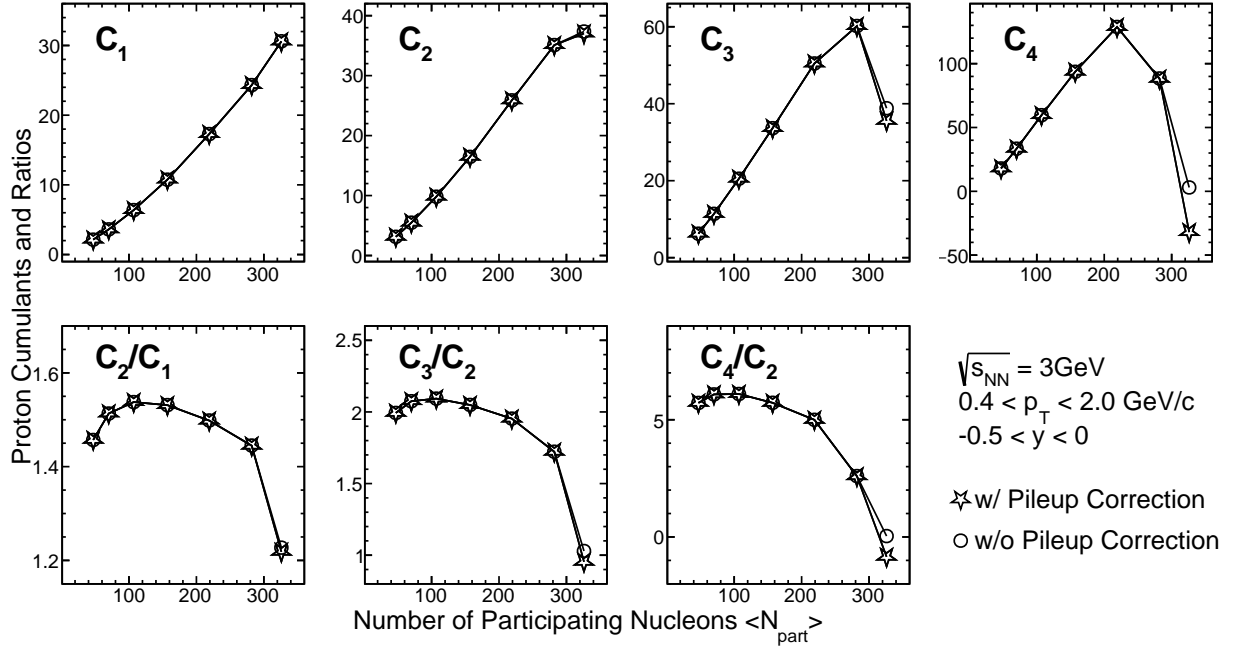
FIG. 2. Centrality dependence of cumulants and cumulant ratios of proton multiplicity distributions for Au+Au collisions at $\sqrt{s_{\mathrm{NN}}} = 3.0$ GeV. Black stars are shown with pile-up correction while black circles are not.

volume fluctuation correction (VFC) method [6] is proposed to deal with this effect in cumulants calculation. The VFC method assumes that the measured particle multiplicity contains contributions from independent participating nucleons. With knowledge of participants distribution, the fluctuation of the volume is removed. Figure 3 shows the proton cumulants and ratios up to 4th order. The squares show the cumulants without the volume fluctuation correction applied. The triangles and circles represent the cumulants with the volume fluctuation correction applied using correction parameters from UrQMD and Glauber model, respectively. The C_1 values are not affected by volume fluctuations. The effect of the correction is highly dependent on the choice of model.
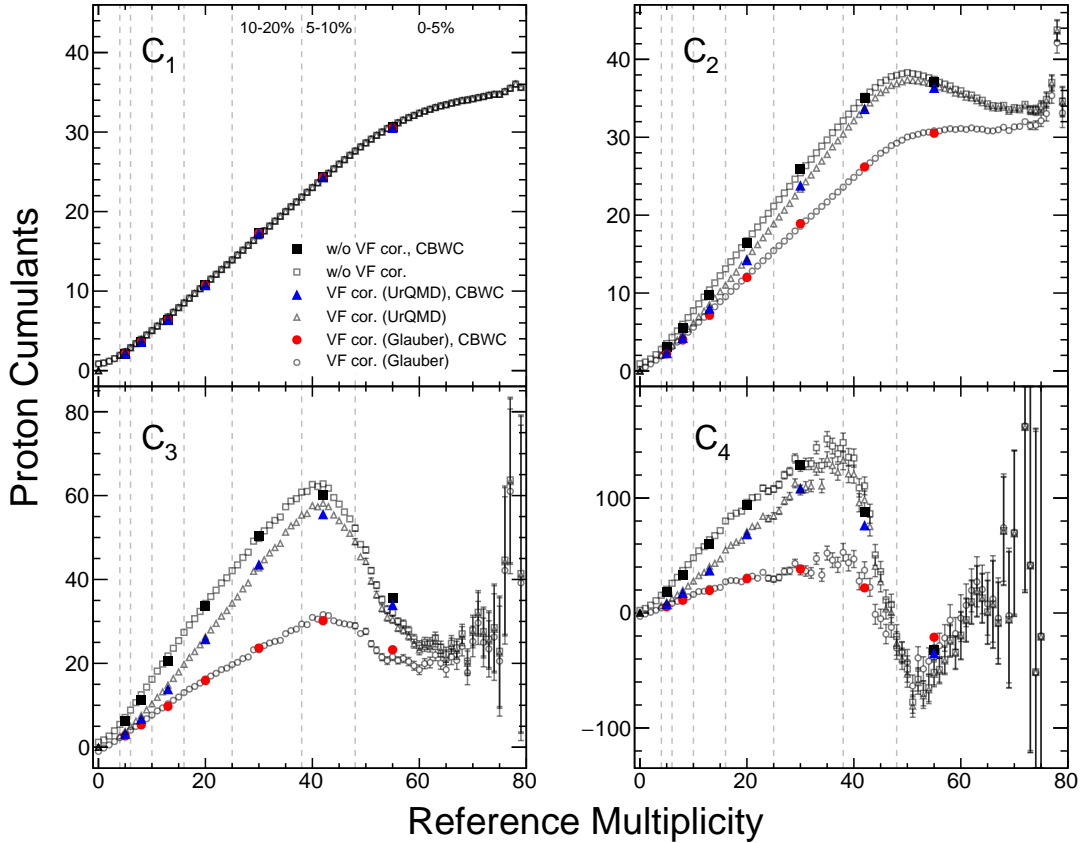
FIG. 3. Centrality dependence of cumulants of proton multiplicity distributions for Au+Au collisions at $\sqrt{s_{\mathrm{NN}}} = 3.0$ GeV. CBWC is applied for all solid markers. VFC is applied as well for all triangles and circles, where the correction parameters are taken from UrQMD and Glauber model, respectively. Statistical uncertainties are shown in bars.

IV. STATISTICAL BASELINE FOR AU+AU COLLISIONS AT $\sqrt{s_{\mathrm{NN}}} = 3.0$ GEV

In the previous STAR Beam Energy Scan (BES) [7], the cumulant ratios of protons in Au+Au peripheral collisions agreed with the Poisson baseline in which all cumulant ratios are equal to one. However, in the Au+Au collisions at $\sqrt{s_{\mathrm{NN}}} = 3.0$ GeV, the cumulants of protons in peripheral collisions are above unity. Figure 4 shows the centrality dependence of the protons cumulants and cumulant ratios fitted with a Negative Binomial Distribution (NBD). As can be seen, the NBD is a more appropriate baseline than the Poisson for the Au+Au collisions at $\sqrt{s_{\mathrm{NN}}} = 3.0$ GeV.
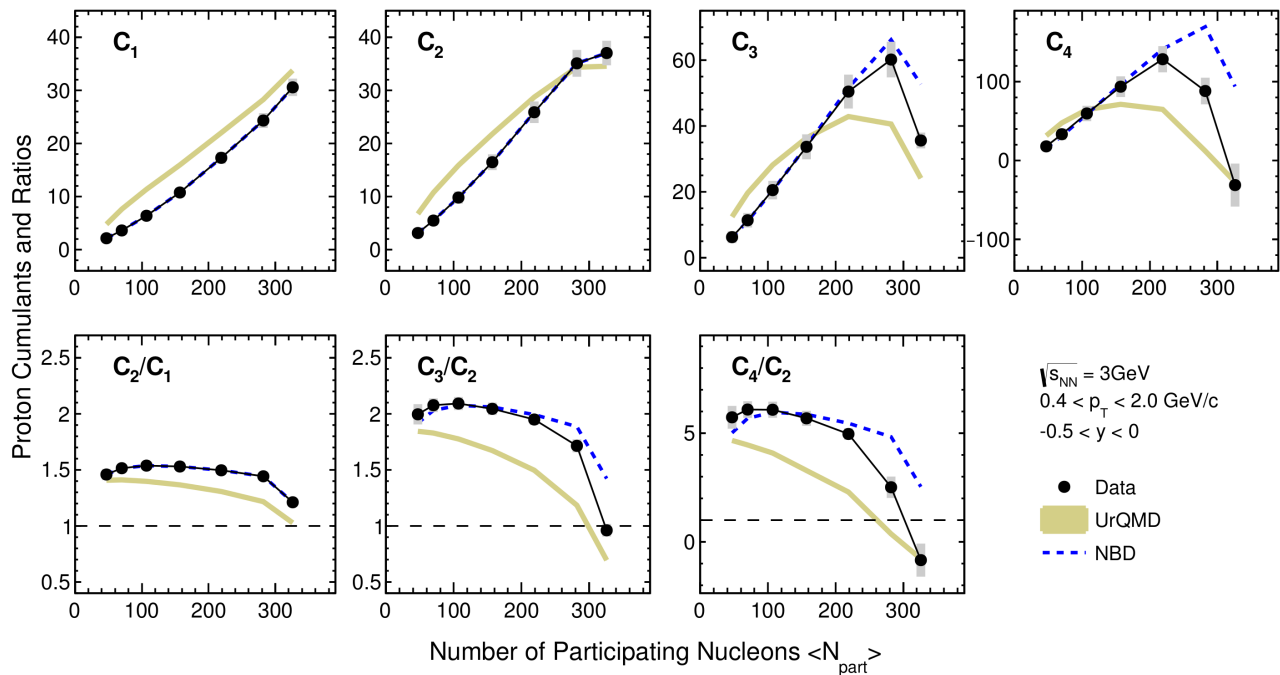
FIG. 4. Centrality dependence of cumulants and cumulant ratios of proton multiplicity distributions for Au+Au collisions at $\sqrt{s_{\mathrm{NN}}} = 3.0$ GeV. Cumulants and ratios are compared to a Negative Binomial distribution (NBD) and UrQMD. NBD is fitted to C_1 and C_2. Systematic uncertainties are shown in gray bars.

V. ACCEPTANCE WINDOW

The analysis is performed in the asymmetric kinematic acceptance of $-0.5 < y < 0$ and $0.4 < p_{\mathrm{T}} < 2.0$ GeV/c. In Fig. 5, the acceptance window is reduced to $-0.1 < y < 0$ and $0 < y < 0.1$. As expected, the forward and backward rapidity windows around mid-rapidity agree.
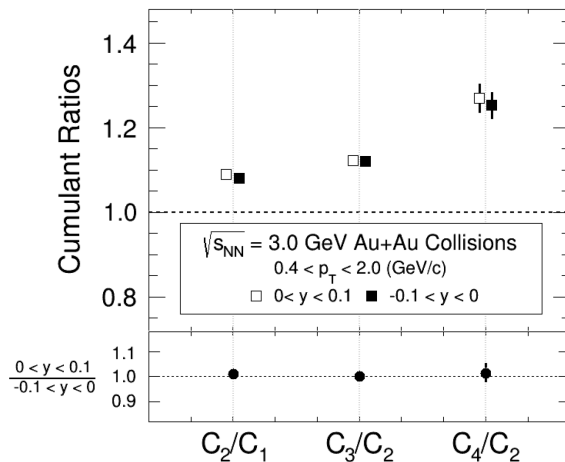

FIG. 5. Cumulant ratios of proton multiplicity distribution from top 0-5% Au+Au collisions at $\sqrt{s_{\mathrm{NN}}} = 3.0$ GeV. Ratios are shown for $0 < y < 0.1$ and $-0.1 < y < 0$ by open and closed squares, respectively. The ratio of using two different acceptance windows are shown below the plot. Statistical uncertainties are represented by black bars.

In the paper, the rapidity dependence is varied from $-0.2 < y < 0$ to $-0.5 < y < 0$ in a fixed transverse momentum of $0.4 < p_{\mathrm{T}} < 2.0$ GeV/c. Figure 6 depicts the rapidity dependence extended to $-0.9 < y < 0$ in a fixed transverse momentum of $0.4 < p_{\mathrm{T}} < 2.0$ GeV/c.
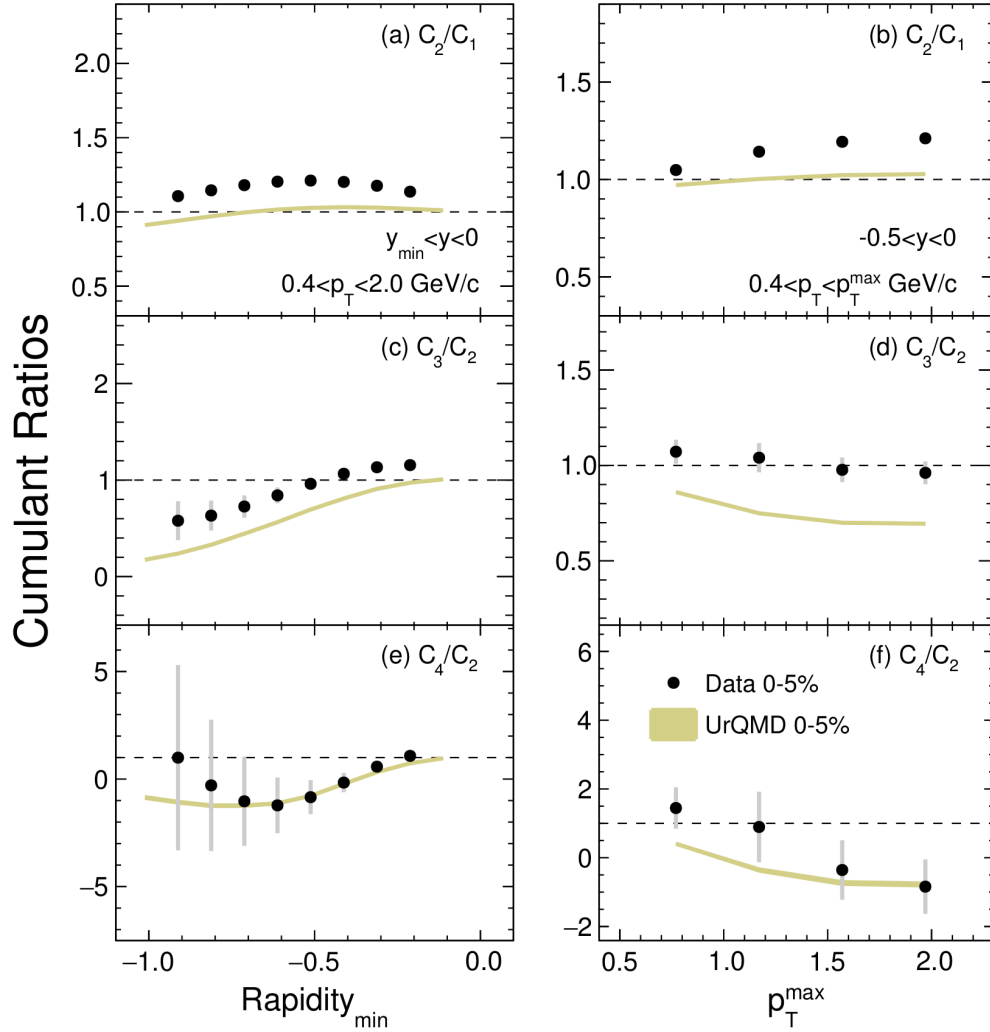
FIG. 6. The transverse-momentum and rapidity dependence of cumulant ratios of proton multiplicity distributions for the most central (0-5%) Au+Au collisions at $\sqrt{s_{\rm NN}} = 3.0$ GeV. In the left panels, the rapidity window is varied from $y_{\rm min} < y < 0$ in the nominal analysis window of $0.4 < p_{\rm T} < 2.0$ GeV/c. In the right panels, the $p_{\rm T}$ is varied from $0.4 < p_{\rm T} < p_{\rm T}^{\rm max}$ GeV/c while the rapidity of the analysis window is fixed to $-0.5 < y < 0$. Systematic uncertainties are represented by gray bars. UrQMD simulation results for the top 0-5% are shown by gold bands.

VI. EFFICIENCY CORRECTION

In this analysis, the detector efficiency is corrected with a "track-by-track" efficiency correction, as outlined in [8]. The correction requires the detector efficiency as function of kinematic acceptance in both the STAR Time Projection Chamber (TPC) and Time of Flight detector (TOF). Figure 7 shows a 2D histogram of the detector efficiency of the TPC and TOF.
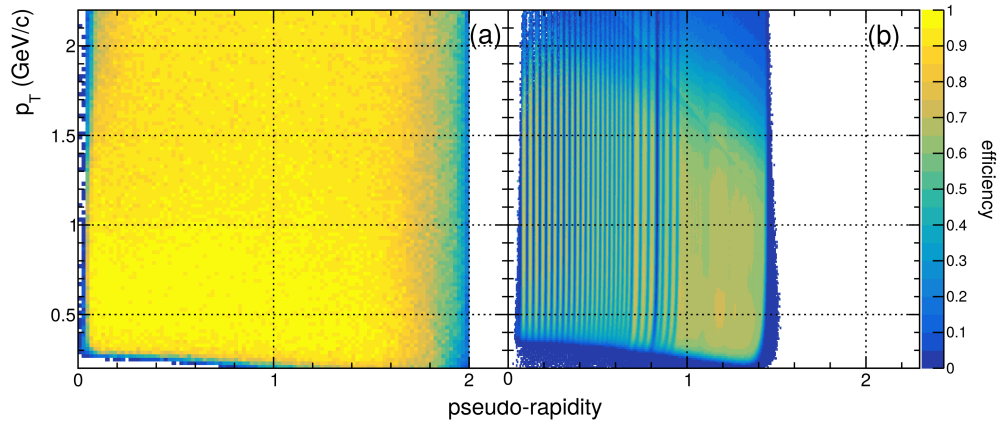
FIG. 7. Left panel (a): The TPC efficiency heat map as a function of transverse momentum and pseudo-rapidity. The efficiency map is generated using a detector model simulation. Right panel (b): The TOF efficiency heat map as a function of transverse momentum and pseudo-rapidity. The efficiency map is generated by taking the ratio of the number of proton tracks in the TOF and TPC in the data.

[1] S. A. Bass et al., Prog. Part. Nucl. Phys. **41**, 255 (1998), arXiv:nucl-th/9803035.
[2] M. Bleicher et al., J. Phys. G **25**, 1859 (1999), arXiv:hep-ph/9909407.
[3] X. Luo, J. Phys. G **39**, 025008 (2012), arXiv:1109.0593 [physics.data-an].
[4] X. Luo, Phys. Rev. C **91**, 034907 (2015), [Erratum: Phys.Rev.C 94, 059901 (2016)], arXiv:1410.3914 [physics.data-an].
[5] T. Nonaka, M. Kitazawa, and S. Esumi, Nucl. Instrum. Meth. A **984**, 164632 (2020).
[6] P. Braun-Munzinger, A. Rustamov, and J. Stachel, Nucl. Phys. A **960**, 114 (2017), arXiv:1612.00702 [nucl-th].
[7] M. S. Abdallah et al., Phys. Rev. C **104**, 10.1103/physrevc.104.024902 (2021).
[8] X. Luo and T. Nonaka, Phys. Rev. C **99**, 044917 (2019), arXiv:1812.10303v2.